Atmos. Chem. Phys. Discuss., 13, 3247–3278, 2013
www.atmos-chem-phys-discuss.net/13/3247/2013/
doi:10.5194/acpd-13-3247-2013

Atmospheric Chemistry and Physics Discussions

Hygroscopic and chemical characterisation of Po Valley aerosol

J. Bialek[1], M. Dall'Osto[1], P. Vaattovaara[2], J. Ovadnevaite[1], S. Decesari[3], A. Laaksonen[4], and C. O'Dowd[1]

[1]School of Physics and Centre for Climate and Air Pollution Studies, National University of Ireland Galway, University Road, Galway, Ireland
[2]University of Eastern Finland, Department of Applied Physics, 70210, Kuopio, Finland
[3]Institute of Atmospheric Sciences and Climate (ISAC) of the Italian National Research Council (CNR), Via P. Gobetti 101, 40129 Bologna, Italy
[4]Finnish Meteorological Institute, Erik Palménin aukio 1, 00560 Helsinki, Finland

Received: 15 January 2013 – Accepted: 17 January 2013 – Published: 4 February 2013

Correspondence to: J. Bialek (jakub.bialek@nuigalway.ie) and C. O'Dowd (colin.odowd@nuigalway.ie)

Published by Copernicus Publications on behalf of the European Geosciences Union.

Abstract

Continental summer-time aerosol in the Italian Po Valley was characterized in terms of hygroscopic properties and the influence of chemical composition therein. The campaign-average minima in hygroscopic growth factors (HGFs) occurred just before and during sunrise from 03:00–06:00, but more generally, the whole night shows very low hygroscopicity, particularly in the smaller particle sizes. The average HGFs increased from 1.18 for the smallest sized particles (35 nm) to 1.38 for the largest sizes (165 nm) for the lowest HGF period while during the day, the HGF gradually increased to achieve maximum values in the early afternoon hours from 12:00–15:00, reaching 1.32 for 35 nm particles and 1.46 for 165 nm particles. Two contrasting case scenarios were encountered during the measurement period: *Case 1* was associated with westerly air flow moving at a moderate pace and *Case 2* was associated with more stagnant, slower moving air from the north-easterly sector. *Case 1* exhibited low diurnal temporal patterns and was associated with moderate non-refractory aerosol mass concentrations (for 50 % size cut at 1 µm) of the order of 4.5 $\mu g\,m^{-3}$. For *Case 1*, organics contributed typically to 50 % of the mass. *Case 2* was characterized by > 9.5 $\mu g\,m^{-3}$ total mass (< 1 µm) in the early morning hours (04:00), decreasing to ~ 3 $\mu g\,m^{-3}$ by late morning (10:00) and exhibited strong diurnal changes in chemical composition, particularly in nitrate mass but also in total organic mass concentrations. Organic growth factors (OGFs) exhibited a minimum around 15:00, 1–2 h after the peak in HGF. Particles sized 165 nm exhibited moderate diurnal variability in HGF, ranging from 80 % at night to 95 % of "more hygroscopic" growth factors (i.e. GF = 1.35–1.9) around noon. The diurnal changes in HGF progressively became enhanced with decreasing particle size, decreasing from 95 % "more hygroscopic" growth factor fraction at noon to 10 % fraction at midnight, while the "less hygroscopic" growth factor fraction (1.13–1.34) increased from 5 % at noon to > 60 % and the "barely hygroscopic" growth factor fraction (1.1–1.2) increased from less than 2 % at noon to 30 % at midnight. OGFs were generally anti-correlated to HGF and also total organic mass as measured by the aerosol

ACPD
13, 3247–3278, 2013

mass spectrometer due to a high sulphate/organics ratio. Surprisingly, the lowest HGFs occurred for periods when nitrate mass reached peak concentrations. This may suggest formation of organonitrates and organosulphates, which significantly decreased the OGF. Coincident with the peak in nitrate was a peak in Hydrocarbon-like Organic Aerosol (HOA) and Semi-Volatile Oxygenated Organic Aerosol (SV-OOA) and analysis of the HGF probability distribution function (PDF) reveals a transformation of a predominant "More Hygroscopic" (MH) mode with HGF of 1.5 around noon, into two modes, one with a "less hygroscopic" (LH) HGF of 1.26, and another with a "barely hygroscopic" (BH) mode of 1.05. The analysis points to an internal mixture of larger size inorganic species, mainly nitrates, coated with a hydrophobic organic layer which suppresses water uptake. In addition, a new, externally mixed BH ultrafine mode appears and persists through the night.

1 Introduction

Light scattering by aerosol particles affects climate forcing through the direct backscattering of incoming solar radiation back into space. The scattering strongly depends on the aerosol's ability to absorb water (hygroscopicity), which in turn, determines the particles ambient size under a given humidity regime. Additionally, hygroscopicity can determine the particles ability to act as a cloud condensation nucleus (Hänel, 1976; Hegg et al., 1993; Svenningsson et al., 1994; McInnes et al., 1998; McFiggans et al., 2006). The aerosol's hygroscopicity may be expressed as a diameter-based hygroscopic growth factor (HGF, Dennis, 1960) and usually is defined as the ratio of the wet particle diameter at a given relative humidity (usually 90 %) to the dry particle diameter at a given relative humidity (usually below 20 %). HGFs for common atmospheric inorganic salts such as ammonium sulphate and sea salt are 1.8 and 2.2, respectively, while oxidized organic aerosol possess lower HGFs and freshly-emitted non-oxidised primary organics have a HGF close to 1.

ACPD
13, 3247–3278, 2013

Primary organic aerosols emitted directly into the atmosphere undergo transformation during transport due to oxidation and multi-phase chemical processes (Rogge et al., 1993; Kittelson, 1998; Kupiainen and Klimont, 2007; Allan et al., 2010) while secondary material is added both as additional, condensable, mass to existing particles, and through the modification of existing aerosol matter (Jimenez et al., 2009). The secondary formation or modification of condensed matter on pre-existing particles may dramatically change their hygroscopic behaviour (Saxena et al., 1995). Particles, previously hydrophobic, but coated with oxidized organics can start to exhibit activity as CCN and participate in cloud formation. The life-cycle of secondarily formed aerosol, however, is not well understood because of myriads of possible chemical compounds taking part in its creation. This is in contrast with the life cycle of inorganic compounds such as sulphates and nitrates whose properties and sources are well-characterized (Ansari and Pandis, 1999). Additionally, understanding the mixing state of organics and inorganics may be of great importance in describing overall impact of anthropogenic pollution on the climate.

Recent technological developments have advanced our capability to chemically-characterise atmospheric aerosols, particularly so with advances in aerosol mass spectrometry. Aerosol mass spectrometry, in conjunction with statistical analysis tools such as positive matrix factorization (PMF) has improved the capability to distinguish between secondary organic aerosol (SOA) and primary organic aerosol (POA), and, in turn, local and regional sources of OA (Paatero and Tapper, 1994; Schauer et al., 1996; Lee et al., 1999; Zhang et al., 2005; Lanz et al., 2007). There have been many laboratory studies performed on secondary organic aerosol (SOA) formation using the hygroscopic tandem differential mobility analyzer (HTDMA) and the aerosol mass spectrometric techniques coupled together (Gysel et al., 2004; Mochida and Kawamura, 2004; Baltensperger et al., 2005; Ng et al., 2006; Meyer et al., 2009; Stratmann et al., 2010; Duplissy et al., 2011; Massoli et al., 2010). In general, all SOA is found to be slightly hygroscopic, with water uptake less than that of typical inorganic aerosol substances. The aerosol water uptake increases with time early in the experiments for the cycloalkane

ACPD
13, 3247–3278, 2013

SOA, but decreases with time for the biogenic SOA. This behaviour could indicate competing effects between the formation of more highly oxidized polar compounds (more hygroscopic), and formation of longer-chained oligomers (less hygroscopic). All SOA also exhibit a smooth water uptake with RH with no deliquescence or efflorescence (Varutbangkul et al., 2006). However, field applications of HTDMA-AMS tandem have been rather less abundant so far (Gasparini et al., 2004; Mochida et al., 2008; Jurányi et al., 2010; Jones et al., 2011; Raatikainen et al., 2010). Additionally, organic tandem differential mobility analyser (OTDMA) and aerosol mass spectrometric have been successfully used in parallel under field conditions (Jimenez et al., 2009; Raatikainen et al., 2010).

This study presents results from the deployment of an HTDMA, OTDMA and an aerosol mass spectrometer (AMS) to characterize continental aerosol properties during the 2009 EUCAARI intensive field campaign in rural region of Po Valley, as a region strongly influenced by urban and transport generated aerosol pollution.

2 Methods and instrumentation

The HTDMA configuration used during the campaign consisted of two Hauke type differential mobility analysers (DMAs), an aerosol conditioner (heated Gore-Tex humidifier), a CPC 3772 with sample flow of 1 L min^{-1}. Relative humidity (RH) was controlled by a Rotronic RH probes and an Edgetech Dewmaster dew-point chilled mirror sensor. The aerosol sample was given a charge equilibrium by Thermo Systems Inc. (TSI) ^{85}Kr aerosol neutralizer operating at activity of 10 mCi. The sizes measured were as follows: 35 nm, 50 nm, 75 nm, 110 nm, and 165 nm. Scan length for each size was set to 180 s; full scan cycle was taking 15 min and 50 s.

The main principle of operation of the DMA (Knutson and Whitby, 1975; Liu et al., 1978) is to select a narrow band of an aerosol size distribution by applying high voltage to its central rod thus selecting particles with a particular electrical mobility. In this way, a monodisperse aerosol distribution is allowed to pass through the instrument.

ACPD
13, 3247–3278, 2013

For the HTDMA, two DMA are positioned on either side of a humidification conditioner, allowing the humidification of a selected dry particle size followed by characterisation of its humidified size. Since the dry diameter of aerosol is well known (aerosol is dried by 50 tubes Nafion dryer down to 5 % RH prior entering first DMA) by measuring the size of particles exiting second DMA one can calculate hygroscopic growth factor (HGF). The sizing of the wet aerosol is achieved by scanning the electrical mobility of the humidified particles and particles exiting second DMA are counted by the CPC. Sheath to aerosol flow ratio is maintained at 1 : 9 by use of critical orifices on both DMA's sheath flow pumps. In order to be able to dry calibrate the HTDMA, two-way valve is fitted before the dryer to bypass it as needed. Whole setup is controlled by the PC which acts as PID controller for the humidifier and a data processor and logger.

An inversion algorithm has to be applied to the measurement distribution function (MDF) of TDMA measurements to retrieve the GF-PDF's correct shape, to determine the mean GF of the sample and to provide the number fractions of particles in different GF ranges (Gysel et al., 2009). The transfer functions of the DMAs are of finite width and because the TDMA's overall transfer probability depends on the GF of the particles, MDF is smoothed and skewed. Additionally, the MDF may contain signal from multiple charged particles which can pass through first DMA as an equivalent of different size particle with the same electrical mobility. Appropriate "inversion" of the raw measurement data is therefore required in most TDMA applications, in order to recover the actual GF-PDF of the investigated aerosol (Gysel et al., 2009). Details of the kernel calibration, data inversion, and TDMA forward function are described (Gysel et al., 2009).

The working principle of the UFO-TDMA (ultrafine organic tandem differential mobility analyser) (Joutsensaari et al., 2001; Vaattovaara et al., 2005) is similar to the HTDMA except for ethanol being the working fluid rather than water and the particles are brought to a selected sub-saturated ethanol vapour environment where they can grow to a new size in accordance their composition and size. The ratio between the measured size in the second DMA and the size selected in the first DMA is called ethanol

ACPD
13, 3247–3278, 2013

growth factor or organic growth factor (OGF, used in this manuscript). Depending on the chemical composition of the particles, different amounts of ethanol are consumed at a given saturation ratio by the particles. We applied the UFO-TDMA (called OTDMA in the following text) to 50 nm particles. The error estimate of the GF values is smaller than 0.01 for 50 nm particles. The saturation ratio was 81 ± 2 %.

Inorganic particles such as sodium chloride and the ammonium sulphate do not grow (i.e. OGF is 1) in the sub-saturated (S = 82 %–84 %) ethanol vapour while pure ammonium bisulphate or particles containing ammonium bisulphate and sulphuric acid with sulphuric acid mass fraction up to 33 % grow in sub-saturated ethanol vapour when the dry particle diameter is 10 nm or smaller and $S < 84$ % (Vaattovaara et al., 2005). Ammonium bisulphate would grow in 50 nm size to 1.02–1.03 at 81–83 % (Vaattovaara et al., 2005). However, this growth is a minor fraction compared to the total growth factor value observed in this study. More importantly, sulphuric acid or ammonium bisulphate are already neutralized to less acidic form in atmospheric 50 nm size particles and thus their OGF behave like ammonium sulphate in atmospheric conditions. On the other hand, particles composed of biogenic organics (e.g. citric acid or tartaric acid) do grow (i.e. OGF is clearly over 1). Generally, moderately oxidized organic do grow very well. It is also notable that if organic compounds are composed of non-polar compounds or if they are highly aged, they do not grow so well either. The OTDMA and the HTDMA provide complementary information about inorganics and organics to ethanol and water, which can be used to indirectly probe the composition behaviour of the particle phase (Vaattovaara et al., 2009). So far, they have been successfully used in parallel to study the composition and diurnal cycles of 50–100 nm particles in different field conditions (Boy et al., 2004; Petäjä et al., 2005; Tiitta et al., 2010).

Aerosol chemical composition was measured with the Aerodyne Research Inc. aerosol mass spectrometer (AMS) which provides real-time size resolved composition analysis of volatile and semi-volatile particulate matter. Combination of size and chemical analysis of sub-micron aerosol mass loading with fast time resolution makes the AMS unique. The theory of operation is described in Jayne et al. (2000) and Jimenez

ACPD
13, 3247–3278, 2013

et al. (2003, 2006). In summary, the AMS quantifies non-refractory aerosol chemical composition, covering major inorganic species such as ammonium, sulphate, nitrate, etc. plus organic species. The AMS detects composition quantitatively by combining thermal vaporization and electron ionization. Factor analysis of AMS data enables differentiation between different OA types and determination of the oxygen content in OA. POA from fossil fuel combustion and other hydrocarbon-like OA (HOA) and biomass-burning OA (BBOA) can be distinguished as can oxygenated organic aerosol (OOA), low-volatility OOA (LV-OOA), semi-volatile OOA (SV-OOA) and cooking OA (COA). PMF (Ulbrich et al., 2009) was run on both low and high resolution AMS organic data with a focus on a 5 factor solution. The 5 factors are: OOA1, OOA2 (regional), HOA, COA and SV-OOA.

3 Measurements location

Measurements were undertaken at San Pietro Capofiume (SPC), situated near Bologna, Emilia-Romagna, Italy (geographical coordinates: 44°39′0″ North, 11°38′0″ East, Fig. 1). The geographical location of the SPC site makes it ideally situated for anthropogenic pollutions studies.

Both rural and urban influences can be investigated and both sources of aerosol can be elucidated. SPC is situated close to two major Po Valley cities: Bologna 25 km to the south, with over 300 000 inhabitants, heavy industry, and a major transportation hub; and Ferrara 20 km to the north, with 130 000 inhabitants and food and machinery industry. The site itself is surrounded by wheat and corn fields with a small food processing plant 800 m south-east from the station. During the campaign, intensive harvesting activities were performed around the site. This region of Italy is characterized by a dense network of primary and secondary roads. San Pietro Capofiume is situated close to main motorways: A14 Bologna–Rimini 22 km from the site to the south, part of motorway system connecting Milano and Adriatic coast, A13 connecting Bologna–Vanezia, 11 km from the site to the west, and motorway link from A13 to the Adriatic coast, 16 km

ACPD
13, 3247–3278, 2013

to the north. Additionally, long range transport and aged aerosol from distant pollution sources along river Po can be investigated.

4 Meteorological overview

Meteorological conditions in San Pietro Capofiume were characterized by weak wind speed, with prevailing E to SE wind direction for 32 % of the time with ESE being the most frequent sector. The strongest wind speeds registered for this sector was 5–6 $m\,s^{-1}$ but only for a fraction of time (< 1 %). The mean wind speed for this sector was 3.5 $m\,s^{-1}$. Highest wind speeds were recorded for W–WNW sector with maximum around 14 $m\,s^{-1}$ for short duration of time (< 1 %). Mean wind speed for this sector was 6.3 $m\,s^{-1}$. Calm conditions (0–1 $m\,s^{-1}$) amounted to 17 % of total duration of campaign. The highest temperature recorded for duration of campaign was 32 °C on 3 July, lowest temperature recorded was 14.5 °C on 11 July.

Air mass back-trajectories were classified into 6 clusters, but essentially we discriminated between two generic types called "West", reflecting a longer range transport from western Europe and the Atlantic, and types called "PoV", describing a weaker circulation with more regional (Po Valley) component. The analysis of shorter (24 h) back trajectories provides essentially the same results. Data for air mass classification were sourced from HYSPLIT 24 h and 48 h back-trajectories with a 500 m a.s.l. endpoint; local meteorological measurements at the station; radio-soundings at SPC (available at http://weather.uwyo.edu/upperair/sounding.html, station code: 16144); and subjective classification of synoptic weather conditions and satellite images. Deep convective systems affected the circulation in the Po Valley sector around SPC on several days bringing strong thundery showers to the site. The circulation driven by these systems cannot be captured by the back trajectory analysis. Convective rainfalls were registered on 5, 7, 9 and 10 July. The highest rainfall was registered on 9 June with 14 mm falling in 30 min.

ACPD
13, 3247–3278, 2013

4.1 Meteorological overview for the chosen cases

4.1.1 Case 1: 7 July 2009 12:00 to 9 July 2009 12:00

In the afternoon of 7 July the air circulation was Po Valley WNW, captured well by the back trajectories. Showers were recorded at SPC from the precipitating systems travelling eastward over the Po Valley. In the period of 8–9 (until midday) July, "West1" or "West2" circulation were recorded and westerly winds captured by the ground sensors and radio soundings at all heights. Clear sky, turned to scattered clouds later in this period.

4.1.2 Case 2: 9 July 2009 12:00 to 11 July 2009 12:00

From the afternoon of 9 to 11 July lowest T_{max} of the campaign was recorded. The T_{min}, was progressively decreasing and it became more humid. Back trajectories were of types "PoV WNW", but actually the circulation was complex: westerlies persisted at the top of the boundary layer (1500 m a.s.l.), and easterly winds (from the Adriatic) intensified at ground level at the end of this period, especially on 11 July. Precipitating systems developed on the Apennines on 9 July around midday, bringing a lot of rain to Bologna and then to SPC. On 10 July, precipitating systems appeared in the eastern Po Valley with heavy rain in SPC.

5 Results and discussion

HGFs for the whole duration of the campaign are displayed in Fig. 2a where darker colours represent lower growth factors and black dots represent averaged HGF between all sizes per HTDMA scan. During the first part of the campaign (27 June 2009 to 5 July 2009), distinct diurnal variability and generally lower HGFs with minima during night time, reaching less than 1.2, increasing to 1.45 during daytime. The second part of campaign (5 July 2009 to 11 July 2009) shows less variability and higher overall

ACPD
13, 3247–3278, 2013

HGF values, ranging from 1.25 to 1.4. During the last two days, the highest daytime HGF of > 1.5 was achieved; but night time HGFs did not drop below 1.3 as it was the case during the first part of the campaign.

Analysis of the aerosol hygroscopicity for the duration of the campaign allows distinguishing several periods:

- A (28 June–2 July) correspond with the highest overall HGFs recorded along with the highest night-time HGFs.
- B (2 July–4 July) shows the highest amplitude of diurnal variability with the lowest recorded night-time HGFs.
- C (5–6 July) can be described best as a transitory between two distinct periods. It was characterized by a high HGF variability.
- D (7 July–9 July, midday) exhibited the lowest amplitude of the HGF diurnal variation for the campaign.
- E (9 July, afternoon–11 July) was characterized again by a clear diurnal pattern of HGF with moderate amplitude between day and night.
- G (12 July) again exhibited very high day-time HGFs while night-time HGFs remained moderately high.

The average diurnal variation of HGF for the duration of the campaign is shown on Fig. 2b. HGF is extrapolated between the five measured sizes to give overall picture of variation both in size and time. The lowest HGFs occurred just before sunrise in hours 03:00–06:00, but generally, the whole night shows very low hygroscopicity, particularly in the smaller sizes. The HGF increased from 1.18 for the smallest sized particles (35 nm) to 1.38 for the largest sizes (165 nm). During the day, the HGF gradually increases to achieve maximum in the afternoon hours 12:00–15:00. Maximum HGFs achieved were 1.32 for 35 nm particles and 1.46 for 165 nm particles.

ACPD
13, 3247–3278, 2013

5.1 Diurnal variability – case studies

Two clear types of diurnal patterns were evident and are chosen for more detailed analysis. One case type was characterized by low diurnal variability while the second case was characterized by a strong diurnal pattern. The HTDMA HGF-probability distribution function (PDF) was integrated to create 4 distinctive aerosol mixing fractions (Swietlicki et al., 2008): a barely hygroscopic fraction with HGF 1–1.12 (BH); a less hygroscopic fraction with HGF 1.125 – 1.34 (LH); a more hygroscopic fraction with HGF 1.345–1.87 (MH); and sea-salt-like fraction with HGF 1.875 and above (SS, wasn't seen in this study).

5.1.1 Case 1, period D: 7 July 2009 12:00 to 9 July 2009 12:00 (Fig. 3)

Temperature started to rise from 05:00 and reached maximum around of 28 °C around noon. A small minimum was caused by convective cloud which started to appear in late morning. The decrease was slowed down by the heat capacity of the ground and its long wave radiation back into the atmosphere. The minimum value of temperature, 19 °C, was recorded around 04:00. Westerly back trajectories during this period suggest advection of relatively fresher air masses (passing over the mountains). Total (AMS-derived) non-refractory aerosol mass concentrations peaked at 5 $\mu g\,m^{-3}$ in the early afternoon, while minimum of 3 $\mu g\,m^{-3}$ was achieved at midnight and shortly after sunrise. A diurnal pattern in the individual AMS mass components wasn't clearly visible either and very low nitrate mass level was observed (less than 0.1 $\mu g\,m^{-3}$ through most of the day with small peak around 20:00 – 0.7 $\mu g\,m^{-3}$). During 24 h contributions of each AMS component was relatively stable with organics dominating the mass contribution, peaking at 2.5 $\mu g\,m^{-3}$. In terms of percentage contribution to total AMS-derived mass, organics contributed 55 %, sulphate 30 %, ammonium 10 % and nitrate 5 %. Organic concentration had three weak maxima during the day: 2.05 $\mu g\,m^{-3}$ around 04:00, 2.55 $\mu g\,m^{-3}$ at 14:00 and 2.5 $\mu g\,m^{-3}$ at 19:00. The minimum for organics was observed 1.45 $\mu g\,m^{-3}$ around 13:00. The sulphate maximum of 2 $\mu g\,m^{-3}$ was recorded around

ACPD
13, 3247–3278, 2013

13:00, while the minimum of 0.6 $\mu g\,m^{-3}$ was recorded midnight. Ammonium followed sulphate and its maximum of 0.7 $\mu g\,m^{-3}$ was recorded at 13:00 while a minimum of 0.3 $\mu g\,m^{-3}$ was encountered at midnight. The AMS PMF analysis reveals a HOA contribution of 5–20 % with peak contributions occurring at 07:00. COA contributes less that 5 % while OOA2 accounts for 20–45 % and OAA1 up to 40 %.

In terms of HGFs, the larger sized particles (165 nm) possess the highest HGFs with 75–80 % contributions from the MH GF and 5–20 % from BH HGFs. As smaller particles are considered, the MH HGF component progressively reduces to between 20–50 % fraction of total particles in the 35 nm size range while the LH HGF component to fraction of 25–60 %. The minimum in growth factor occurs at 03:00–04:00, corresponding to a relative peak in the OGF of 1.13. Second and third peaks, both of the order of 1.125, are also seen at 10:00 and 12:00. The BH HFG tracks the HOA signal the closest. OGF diurnal variation seems to follow roughly AMS organic mass load, while being anti-correlated with the HGF.

A semi-volatile fraction (SV OOA) is visible during whole day in stable concentrations with only slightly higher contributions during the night. This fraction comes from partial oxidation of organics and is represented well by diurnal variations of LH HGF group in 110 nm particle size range. It is also worth mentioning that so called "Cooking Aerosol" (COA) factor concentration is steadily increasing from around 18:00 although its hygroscopicity and solubility in the ethanol is too similar either to HOA or SV-OOA to be visible as changes in HGF. At the same time, OGFs are most similar to SV-OOA and OO1. Generally, OGFs follow the total organic mass trend while sulphate/organics and sulphate/nitrate ratios changed only by a small value. Regional OOA2 concentration dominated at the measurement site. The peak of concentration for this factor was recorded around noon and slowly decreased over time maintaining its dominance till late evening. OOA1 followed closely OOA2 peaking around noon but also exhibiting a secondary peak in the evening rush hour time.

The average 50 nm OGF and HGF is plotted against the total AMS organic mass and the HGF-PDF in Fig. 4 where OGF increases when moderately aged aerosol is

ACPD
13, 3247–3278, 2013

present, especially when HGF reaches values around 1.2. The PDF illustrates a predominant HGF mode between 1.25 and 1.35 throughout the period, with two additional GF modes, one at 1.45 and one at 1.05, occurring at night-time. Overall, the OGFs and HGFs are consistent with the relative proportions of organics, sulphates and nitrates, along with the oxygenated level of the organics.

5.1.2 Case 2, period E: 9 July 2009 12:00 to 11 July 2009 12:00 (Fig. 5)

For this case, temperature was initially quite similar to *Case 1* increasing from 05:00 and peaking around noon. In the afternoon, fast development of convective clouds cause the overcast and temperature decrease. This was further accelerated by the rain showers. Maximum of 26 °C was recorded around 14:00, and a minimum of 15 °C was recorded at 04:00. In contrast to *Case 1*, much higher levels of aerosol pollution was observed with peak concentrations of AMS-derived non-refractory mass exceeding 9 $\mu g\,m^{-3}$ around 04:00, reducing to $\sim 3\,\mu g\,m^{-3}$ at 09:00–10:00. A daytime peak of $\sim 4\,\mu g\,m^{-3}$ is seen at 13:00. The strong diurnal signal is primarily driven by the nitric acid temporal trend, but is also notably influenced by the organic contribution. This also makes possible the formation of organonitrates during night time when nitrate and organic concentrations are high. Thermodymically, nitric acid is not expected to be present in ultrafine size (i.e. < 100 nm) particles. This is supported by the changing HGF fractions as the function of particles size in Fig. 5 because organonitrates in polluted conditions have reasonable high HGF values compared to organics in more clean conditions (Vaattovaara et al., 2009). Generally, the formation of organonitrates is expected to be probable, especially in the environment with high load of both nitrates and organics. Typically, that kind of high load conditions are observed during night time at SPC station.

The highest variance was exhibited in nitrate mass which ranged from 4 $\mu g\,m^{-3}$ at 04:00 to less than 0.1 $\mu g\,m^{-3}$ throughout the rest of the day. Total organic concentration was the highest during night-time and its maximum also corresponds with the maximum of nitrate, 3.2 $\mu g\,m^{-3}$, occurring around 04:00 (see also Fig. 8). Minimum

ACPD
13, 3247–3278, 2013

concentration of organics was recorded around 10:00 and slowly increased thereafter. Sulphate followed a different, flatter pattern, with a minimum of 0.7 $\mu g\,m^{-3}$ around 08:00 and maximum of 1.5 $\mu g\,m^{-3}$ around noon. Ammonium exhibited two maxima accordingly to nitrate and sulphate maxima ranging from 1.5 $\mu g\,m^{-3}$ at 04:00 to its minimum of 0.3 $\mu g\,m^{-3}$ at 08:00.

HOA accumulation was quite pronounced after midnight and was accelerated during the morning rush hour period. However, there is no evidence of the evening rush hour leading to HOA accumulation. This factor is also very well visible in HGF data as BH fraction which follows closely HOA's diurnal pattern in all measured sizes. COA concentration increases from around 17:00 and remains stable during the night and seems to correspond closely to the BH HGF, adding to the HOA contribution. Similar patterns are seen for sizes in range of 35–110 nm. The SV-OOA factor concentration started to increase from around 14:00 and reached a maximum around midnight. This factor dominates the HGF LH fraction. The diurnal evolution of LH follows SV-OOA very closely in 35–75 nm size ranges.

Both OOA2 and OOA1 had equal contribution to total OOA from noon till late evening. After midnight however, regional OOA1 contribution increased while local OOA2 decreased during the night.

The MH fraction of HGFs exhibited higher diurnal variability in size range from 35 nm to 75 nm, with the strongest pattern seen in the smallest sizes. For larger particle sizes of 110 nm and 165 nm, a less strong diurnal pattern was seen, with an overall maximum through all sizes recorded around noon. Interestingly, two minima were also recorded in MH fraction: in late evening and again in the morning hours. A diurnal cycle was less evident in the somewhat unbalanced OGF signal during this period. However, a clear minimum of 1.09 was seen in the mid-afternoon. This minimum was related to the increase of sulphate, OOA1 and OOA2. Because OGF values decrease so strongly and HGF values increase so rapidly, the formation of organosulphates is the most probable explanation for the 50 nm OGF and HGF behaviour. This is due to a previous atmospheric observation (Vaattovaara et al., 2009) that in the case of combined sulphates

ACPD
13, 3247–3278, 2013

and organics, OGF values decrease and HGF values increase. The minimum was followed rapidly by a peak of 1.15 at 17:00 due to local change in the air mass with less sulphate, OOA1 and OOA2, thus less organosulphates but more ethanol soluble semi-volatile OOA. This effect was enhanced by a quick temperature drop from 26 °C to 19 °C. Another OGF peak of 1.13 was just before midnight due to additional increase of SV-OOA fraction. Overall aerosol ethanol solubility is higher during the late afternoon and night hours. The minima in the OGF seem to anti-correlate with the MH HGF fraction for sizes 35–110 nm. Higher COA concentrations seem to suppress aerosol solubility in ethanol.

Figure 6 shows that the OGF mostly anti-correlates with the AMS total organic mass load. This behavior seems to be related to a high sulphate/organics ratio. OGFs stays high as long as group of particles with mean HGF from 1.2 to 1.3 predominates and it is lower when hydrophobic group predominates and 1.3 HGF group decreases in concentration. Occurrence of particle group with very low HGF corresponds well with AMS organic load. The OGF is generally anti-correlated to HGF. Analysis of the HGF-PDF reveals a higher degree of variability in the mean HGF with mean HGF of 1.4 through midday, reducing to 1.2 at night. During early evening through to late morning, a low HGF mode at 1.05 is also evident and persistent.

Figure 7 shows time-slice PDFs extracted for each of the HGF sizes at 04:00–05:00 (i.e. the nitrate peak, total mass peak, and HGF minimum) and at 12:00–13:00 (the OGF minimum and HGF peak) while Fig. 8 shows AMS nitrates mass concentration for both morning and noon time periods. While not being quantitatively reliable, careful calculation of number concentration of particles from AMS mass concentration can give a rough idea of size regimes in which both AMS and HTDMA overlap. Analysis of nitrates number distribution in mobility equivalent diameter (Fig. 9) reveals that the majority of particles are represented by 50 nm–110 nm size range, which overlaps both HTDMA and OTDMA measurement regime. For 50 nm particles, during the nitrate peak, two strong HGF modes are seen at 1.04 and 1.2, with a third, less pronounced peak at 1.36. This contrasts to the noontime predominant single peak at 1.44

ACPD
13, 3247–3278, 2013

and a significantly less evident HGF mode at 1.14. For 110 nm sized particles, the HGF PDF during the nitrate peak is again tri-modal, with a primary mode at 1.4, a secondary mode at 1.04, and a third, minor, peak at 1.26. This contrasts to the noontime primary peak of 1.5 and secondary minor peak of 1.26. The general trend is twofold: (1) there is a notable reduction in the HGF associated with the MH mode, with a reduction in HGF from ∼ 1.5 to ∼ 1.26; and (2) there is the appearance of at least one BH mode.

6 Conclusions

A HTDMA, OTDMA and AMS were deployed in the Po Valley San Pietro Capofiume research station to characterize water and ethanol uptake by the aerosol associated with polluted continental air and how these properties are influenced by the aerosol chemical composition. The average diurnal variation of HGF for the duration of the campaign revealed the lowest HGFs occurring just before sunrise in hours 03:00–06:00 and in the smallest sizes. HGF increased from 1.18 for 35 nm particles to 1.38 for 165 nm sized particles. During the day, the HGF gradually increased to achieve maximum in the afternoon hours 12:00–15:00. Maximum HGFs achieved were 1.32 for 35 nm particles and 1.46 for 165 nm particles. Diurnal behaviour of HGF and OGF values suggest the presence of organonitrates in particles during night time and the presence of organosulphates during day time.

Two cases were examined in close detail in terms of the influence of chemical composition on HGF. One case type was characterized by moderate levels of pollution and with organic matter dominating the aerosol mass. This case illustrated little diurnal variability in relative contributions of different aerosol types, HGF, or OGF. The strongest pattern was a reduction in the MH mode from approximately 80 % in 165 nm sized particles to 20–40 % in 35 nm sized particles while the LH mode contribution increased from less than 5 % to more than 30 % over the same size range. For this case, organic mass contributed approximately 50 % of the total non-refractory mass. OGF values positively followed the trends of the OOAs. In contrast to *Case 1*, the second selected

ACPD
13, 3247–3278, 2013

case had more than double the aerosol mass and exhibited a strong diurnal pattern, particularly for nitrates and also for organic mass, both of which peaked in the early morning as peak mass concentration exceeded 9.5 $\mu g\,m^{-3}$, making also the formation of organonitrates more probable. Particularly in the smallest sized particles, a strong diurnal signal was seen in the HGFs with peak HGFs occurring around noon and minima occurring around midnight. Despite nitrate mass peaking at 4 $\mu g\,m^{-3}$ around 04:00, the MH HGF reached its minimum value and both the BH and LH factors reached their maximum values. OGFs were anti-correlated with HGFs, as to be expected, but were also more generally anti-correlated with total organic aerosol mass and OOAs, in particular, the OOA1 due to high and varying sulphate/organics and nitrate/organics ratios and, consequently, organosulphate and organonitrate formation. In the evening, the higher OGFs were mainly due the increase of the SV-OOA fraction. Additionally, the OGFs positively correlated with the HOA factor. Analysis of the HGF-PDF reveals a transformation of a predominant MH mode with HGF of 1.5 around noon, into two modes, one with a HGF of 1.26 (i.e. LH) and another with a HGF of 1.05 (BH). The analysis points to an internal mixture of inorganic species, mainly nitrates, coated with a hydrophobic organic layer which suppresses water uptake. In addition, a new, externally mixed BH mode appears and is persistent.

Acknowledgements. This work was supported by the FP6 EUCAARI Integrated Project, Irelands Higher Education Authority Programme for Research in Third Level Institutes (4) project Environment and Climate: Impact at Responses, and the Center of Excellence of Finnish Academy.

References

Allan, J. D., Williams, P. I., Morgan, W. T., Martin, C. L., Flynn, M. J., Lee, J., Nemitz, E., Phillips, G. J., Gallagher, M. W., and Coe, H.: Contributions from transport, solid fuel burning and cooking to primary organic aerosols in two UK cities, Atmos. Chem. Phys., 10, 647–668, doi:10.5194/acp-10-647-2010, 2010.

ACPD
13, 3247–3278, 2013

Ansari, A. S. and Pandis, S. N.: Prediction of multicomponent inorganic atmospheric aerosol behavior, Atmos. Environ., 33, 745–757, 1999.

Baltensperger, U., Kalberer, M., Dommen, J., Paulsen, D., Alfarra, M. R., Coe, H., Fisseha, R., Gascho, A., Gysel, M., Nyeki, S., Sax, M., Steinbacher, M., Prevot, A. S. H., Sjogren, S., Weingartner, E., and Zenobi, R.: Secondary organic aerosols from anthropogenic and biogenic precursors, Faraday Discuss., 130, 265–278, 2005.

Boy, M., Petäjä, T., Dal Maso, M., Rannik, Ü., Rinne, J., Aalto, P., Laaksonen, A., Vaattovaara, P., Joutsensaari, J., Hoffmann, T., Warnke, J., Apostolaki, M., Stephanou, E. G., Tsapakis, M., Kouvarakis, A., Pio, C., Carvalho, A., Römpp, A., Moortgat, G., Spirig, C., Guenther, A., Greenberg, J., Ciccioli, P., and Kulmala, M.: Overview of the field measurement campaign in Hyytiälä, August 2001 in the framework of the EU project OSOA, Atmos. Chem. Phys., 4, 657–678, doi:10.5194/acp-4-657-2004, 2004.

Dennis, W. L.: The growth of hygroscopic drops in a humid air stream, Discuss. Faraday Soc., 30, 78–85, 1960.

Duplissy, J., DeCarlo, P. F., Dommen, J., Alfarra, M. R., Metzger, A., Barmpadimos, I., Prevot, A. S. H., Weingartner, E., Tritscher, T., Gysel, M., Aiken, A. C., Jimenez, J. L., Canagaratna, M. R., Worsnop, D. R., Collins, D. R., Tomlinson, J., and Baltensperger, U.: Relating hygroscopicity and composition of organic aerosol particulate matter, Atmos. Chem. Phys., 11, 1155–1165, doi:10.5194/acp-11-1155-2011, 2011.

Gasparini, R., Li, R., and Collins, D. R.: Integration of size distributions and size-resolved hygroscopicity measured during the Houston Supersite for compositional categorization of the aerosol, Atmos. Environ., 38, 3285–3303, 2004.

Gysel, M., Weingartner, E., Nyeki, S., Paulsen, D., Baltensperger, U., Galambos, I., and Kiss, G.: Hygroscopic properties of water-soluble matter and humic-like organics in atmospheric fine aerosol, Atmos. Chem. Phys., 4, 35–50, doi:10.5194/acp-4-35-2004, 2004.

Gysel, M., McFiggans, G. B., and Coe, H.: Inversion of tandem differential mobility analyser (TDMA) measurements, J. Aerosol Sci., 40, 134–151, 2009.

Hänel, G.: The Properties of Atmospheric Aerosol Particles as Functions of the Relative Humidity at Thermodynamic Equilibrium with the Surrounding Moist Air, Adv. Geophys., 19, 73–188, 1976.

Hegg, D., Larson, T., and Po-Fat, Y.: A theoretical study of the effect of relative humidity on light scattering by tropospheric aerosols, J. Geophys. Res., 98, 18435–18439, 1993.

ACPD
13, 3247–3278, 2013

Jayne, T. J., Leard, C. D., Zhang, X., Davidovits, P., Smith, A. K., Kolb, E. C., and Worsnop, R. D.: Development of an aerosol mass spectrometer for size and composition analysis of submicron particles, Taylor and Francis, Colchester, UK, 2000.

Jimenez, J. L., Jayne, J. T., Shi, Q., Kolb, C. E., Worsnop, D. R., Yourshaw, I., Seinfeld, J. H., Flagan, R. C., Zhang, X., Smith, K. A., Morris, J. W., and Davidovits, P.: Ambient aerosol sampling using the Aerodyne Aerosol Mass Spectrometer, J. Geophys. Res.-Atmos., 108, 8425, doi:10.1029/2001JD001213, 2003.

Jimenez, J. L., DeCarlo, P. F., Kimmel, J. R., Trimborn, A., Northway, M. J., Jayne, J. T., Aiken, A. C., Gonin, M., Fuhrer, K., Horvath, T., Docherty, K. S., and Worsnop, D. R. Field-deployable, high-resolution, time-of-flight aerosol mass spectrometer, Anal. Chem., 78, 8281–8289, 2006.

Jimenez, J. L., Canagaratna, M. R., Donahue, N. M., Prevot, A. S. H., Zhang, Q., Kroll, J. H., DeCarlo, P. F., Allan, J. D., Coe, H., Ng, N. L., Aiken, A. C., Docherty, K. S., Ulbrich, I. M., Grieshop, A. P., Robinson, A. L., Duplissy, J., Smith, J. D., Wilson, K. R., Lanz, V. A., Hueglin, C., Sun, Y. L., Tian, J., Laaksonen, A., Raatikainen, T., Rautiainen, J., Vaattovaara, P., Ehn, M., Kulmala, M., Tomlinson, J. M., Collins, D. R., Cubison, M. J., Dunlea, E. J., Huffman, J. A., Onasch, T. B., Alfarra, M. R., Williams, P. I., Bower, K., Kondo, Y., Schneider, J., Drewnick, F., Borrmann, S., Weimer, S., Demerjian, K., Salcedo, D., Cottrell, L., Griffin, R., Takami, A., Miyoshi, T., Hatakeyama, S., Shimono, A., Sun, J. Y., Zhang, Y. M., Dzepina, K., Kimmel, J. R., Sueper, D., Jayne, J. T., Herndon, S. C., Trimborn, A. M., Williams, L. R., Wood, E. C., Middlebrook, A. M., Kolb, C. E., Baltensperger, U., and Worsnop, D. R.: Evolution of organic aerosols in the atmosphere, Science, 326, 1525–1529, 2009.

Jones, H. M., Crosier, J., Russell, A., Flynn, M. J., Irwin, M., Choularton, T. W., Coe, H., and McFiggans, G.: In situ aerosol measurements taken during the 2007 COPS field campaign at the Hornisgrinde ground site, Q. J. Roy. Meteorol. Soc., 137, 252–266, 2011.

Joutsensaari, J., Vaattovaara, P., Vesterinen, M., Hämeri, K., and Laaksonen, A.: A novel tandem differential mobility analyzer with organic vapor treatment of aerosol particles, Atmos. Chem. Phys., 1, 51–60, doi:10.5194/acp-1-51-2001, 2001.

Jurányi, Z., Gysel, M., Weingartner, E., DeCarlo, P. F., Kammermann, L., and Baltensperger, U.: Measured and modelled cloud condensation nuclei number concentration at the high alpine site Jungfraujoch, Atmos. Chem. Phys., 10, 7891–7906, doi:10.5194/acp-10-7891-2010, 2010.

ACPD
13, 3247–3278, 2013

Kittelson, D. B.: Engines and nanoparticles: a review, J. Aerosol Sci., 29, 575–588, 1998.
Knutson, E. O. and Whitby, K. T.: Aerosol classification by electric mobility: apparatus, theory, and applications, J. Aerosol Sci., 6, 443–451, 1975.
Kupiainen, K. and Klimont, Z.: Primary emissions of fine carbonaceous particles in Europe, Atmos. Environ., 41, 2156–2170, 2007.
Lanz, V. A., Alfarra, M. R., Baltensperger, U., Buchmann, B., Hueglin, C., and Prévôt, A. S. H.: Source apportionment of submicron organic aerosols at an urban site by factor analytical modelling of aerosol mass spectra, Atmos. Chem. Phys., 7, 1503–1522, doi:10.5194/acp-7-1503-2007, 2007.
Lee, E., Chan, C. K., and Paatero, P.: Application of positive matrix factorization in source apportionment of particulate pollutants in Hong Kong, Atmos. Environ., 33, 3201–3212, 1999.
Liu, B. Y. H., Pui, D. Y. H., and Whitby, K. T.: The aerosol mobility chromatograph: a new detector for sulfuric acid aerosols, Atmos. Environ., 12, 99–104, 1978.
Massoli, P., Lambe, A. T., Ahern, A. T., Williams, L. R., Ehn, M., Mikkilä, J., Canagaratna, M. R., Brune, W. H., Onasch, T. B., Jayne, J. T., Petäjä, T., Kulmala, M., Laaksonen, A., Kolb, C. E., Davidovits, P., and Worsnop, D. R.: Relationship between aerosol oxidation level and hygroscopic properties of laboratory generated secondary organic aerosol (SOA) particles, Geophys. Res. Lett., 37, L24801, doi:10.1029/2010GL045258, 2010.
McFiggans, G., Artaxo, P., Baltensperger, U., Coe, H., Facchini, M. C., Feingold, G., Fuzzi, S., Gysel, M., Laaksonen, A., Lohmann, U., Mentel, T. F., Murphy, D. M., O'Dowd, C. D., Snider, J. R., and Weingartner, E.: The effect of physical and chemical aerosol properties on warm cloud droplet activation, Atmos. Chem. Phys., 6, 2593–2649, doi:10.5194/acp-6-2593-2006, 2006.
McInnes, L., Bergin, M., Ogren, J., and Schwartz, S.: Apportionment of light scattering and hygroscopic growth to aerosol composition, Geophys. Res. Lett., 25, 513–516, 1998.
Meyer, N. K., Duplissy, J., Gysel, M., Metzger, A., Dommen, J., Weingartner, E., Alfarra, M. R., Prevot, A. S. H., Fletcher, C., Good, N., McFiggans, G., Jonsson, Å. M., Hallquist, M., Baltensperger, U., and Ristovski, Z. D.: Analysis of the hygroscopic and volatile properties of ammonium sulphate seeded and unseeded SOA particles, Atmos. Chem. Phys., 9, 721–732, doi:10.5194/acp-9-721-2009, 2009.
Mochida, M. and Kawamura, K.: Hygroscopic properties of levoglucosan and related organic compounds characteristic to biomass burning aerosol particles, J. Geophys. Res.-Atmos., 109, 1–8, 2004.

ACPD
13, 3247–3278, 2013

Mochida, M., Miyakawa, T., Takegawa, N., Morino, Y., Kawamura, K., and Kondo, Y.: Significant alteration in the hygroscopic properties of urban aerosol particles by the secondary formation of organics, Geophys. Res. Lett., 35, L02804, doi:10.1029/2007GL031310, 2008.

Ng, N. L., Kroll, J. H., Keywood, M. D., Bahreini, R., Varutbangkul, V., Flagan, R. C., Seinfeld, J. H., Lee, A., and Goldstein, A. H.: Contribution of first- versus second-generation products to secondary organic aerosols formed in the oxidation of biogenic hydrocarbons, Environ. Sci. Technol., 40, 2283–2297, 2006.

Paatero, P. and Tapper, U.: Positive matrix factorization: a non-negative factor model with optimal utilization of error estimates of data values, Environmetrics, 5, 111–126, 1994.

Petäjä, T., Kerminen, V.-M., Hämeri, K., Vaattovaara, P., Joutsensaari, J., Junkermann, W., Laaksonen, A., and Kulmala, M.: Effects of SO_2 oxidation on ambient aerosol growth in water and ethanol vapours, Atmos. Chem. Phys., 5, 767–779, doi:10.5194/acp-5-767-2005, 2005.

Raatikainen, T., Vaattovaara, P., Tiitta, P., Miettinen, P., Rautiainen, J., Ehn, M., Kulmala, M., Laaksonen, A., and Worsnop, D. R.: Physicochemical properties and origin of organic groups detected in boreal forest using an aerosol mass spectrometer, Atmos. Chem. Phys., 10, 2063–2077, doi:10.5194/acp-10-2063-2010, 2010.

Rogge, W. F., Hildemann, L. M., Mazurek, M. A., Cass, G. R., and Simoneit, B. R. T.: Sources of fine organic aerosol, 2: noncatalyst and catalyst-equipped automobiles and heavy-duty diesel trucks, Environ. Sci. Technol., 27, 636–651, 1993.

Saxena, P., Hildemann, L. M., McMurry, P. H., and Seinfeld, J. H.: Organics alter hygroscopic behavior of atmospheric particles, J. Geophys. Res., 100, 18755–18770, 1995.

Schauer, J. J., Rogge, W. F., Hildemann, L. M., Mazurek, M. A., Cass, G. R., and Simoneit, B. R. T.: Source apportionment of airborne particulate matter using organic compounds as tracers, Atmos. Environ., 30, 3837–3855, 1996.

Stratmann, F., Bilde, M., Dusek, U., Frank, G. P., Hennig, T., Henning, S., Kiendler-Scharr, A., Kiselev, A., Kristensson, A., Lieberwirth, I., Mentel, T. F., Pöschl, U., Rose, D., Schneider, J., Snider, J. R., Tillmann, R., Walter, S., and Wex, H.: Examination of laboratory-generated coated soot particles: an overview of the LACIS Experiment in November (LExNo) campaign, J. Geophys. Res.-Atmos., 115, D11203, doi:10.1029/2009JD012628, 2010.

Svenningsson, B., Hansson, H. C., Wiedensohler, A., Noone, K., Ogren, J., Hallberg, A., and Colvile, R.: Hygroscopic growth of aerosol particles and its influence on nucleation

ACPD
13, 3247–3278, 2013

scavenging in cloud: experimental results from Kleiner Feldberg, J. Atmos. Chem., 19, 129–152, 1994.

Swietlicki, E., Hansson, H. C., Hämeri, K., Svenningsson, B., Massling, A., McFiggans, G., McMurry, P. H., Petäjä, T., Tunved, P., Gysel, M., Topping, D., Weingartner, E., Baltensperger, U., Rissler, J., Wiedensohler, A., and Kulmala, M.: Hygroscopic properties of submicrometer atmospheric aerosol particles measured with H-TDMA instruments in various environments – a review, Tellus B, 60, 432–469, 2008.

Tiitta, P., Miettinen, P., Vaattovaara, P., Joutsensaari, J., Petäjä, T., Virtanen, A., Raatikainen, T., Aalto, P., Portin, H., Romakkaniemi, S., Kokkola, H., Lehtinen, K. E. J., Kulmala, M., and Laaksonen, A.: Roadside aerosol study using hygroscopic, organic and volatility TDMAs: characterization and mixing state, Atmos. Environ., 44, 976–986, 2010.

Ulbrich, I. M., Canagaratna, M. R., Zhang, Q., Worsnop, D. R., and Jimenez, J. L.: Interpretation of organic components from Positive Matrix Factorization of aerosol mass spectrometric data, Atmos. Chem. Phys., 9, 2891–2918, doi:10.5194/acp-9-2891-2009, 2009.

Vaattovaara, P., Räsänen, M., Kühn, T., Joutsensaari, J., and Laaksonen, A.: A method for detecting the presence of organic fraction in nucleation mode sized particles, Atmos. Chem. Phys., 5, 3277–3287, doi:10.5194/acp-5-3277-2005, 2005.

Vaattovaara, P., Petäjä, T., Joutsensaari, J., Miettinen, P., Zaprudin, B., Kortelainen, A., Heijari, J., Yli-Pirilä, P., Aalto, P., Worsnop, D. R., and Laaksonen, A.: The evolution of nucleation- and Aitken-mode particle compositions in a boreal forest environment during clean and pollution-affected new-particle formation events, Boreal Environ. Res., 14, 662–682, 2009.

Varutbangkul, V., Brechtel, F. J., Bahreini, R., Ng, N. L., Keywood, M. D., Kroll, J. H., Flagan, R. C., Seinfeld, J. H., Lee, A., and Goldstein, A. H.: Hygroscopicity of secondary organic aerosols formed by oxidation of cycloalkenes, monoterpenes, sesquiterpenes, and related compounds, Atmos. Chem. Phys., 6, 2367–2388, doi:10.5194/acp-6-2367-2006, 2006.

Zhang, Q., Worsnop, D. R., Canagaratna, M. R., and Jimenez, J. L.: Hydrocarbon-like and oxygenated organic aerosols in Pittsburgh: insights into sources and processes of organic aerosols, Atmos. Chem. Phys., 5, 3289–3311, doi:10.5194/acp-5-3289-2005, 2005.

ACPD
13, 3247–3278, 2013

Fig. 1. Po Valley is bordered by the Alps to the north and west, by the forefront of Apennines Mountains to the south and the Adriatic Sea to the east. San Pietro Capofiume site (SPC) is marked with A on the map (sourced from Tele Atlas 2011).

ACPD
13, 3247–3278, 2013

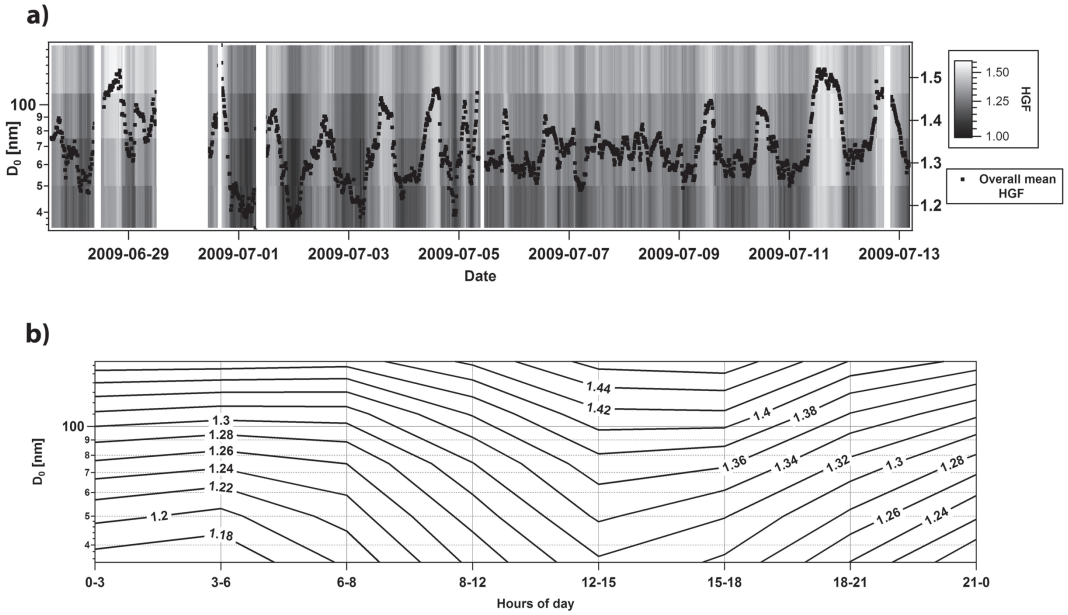

Fig. 2. (a) Size resolved HGF and mean HGF for whole duration of the campaign, **(b)** size resolved diurnal variability of HGF for whole campaign.

ACPD
13, 3247–3278, 2013

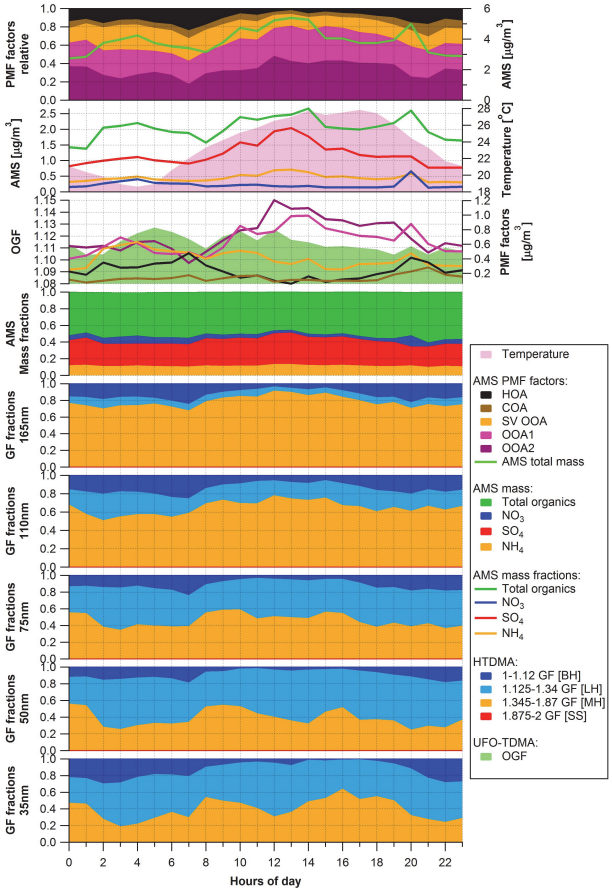

Fig. 3. Diurnal pattern for HGF, OGF, AMS mass fractions, PMF factors and temperature. Period: 7 July 2009 12:00 to 9 July 2009 12:00.

ACPD
13, 3247–3278, 2013

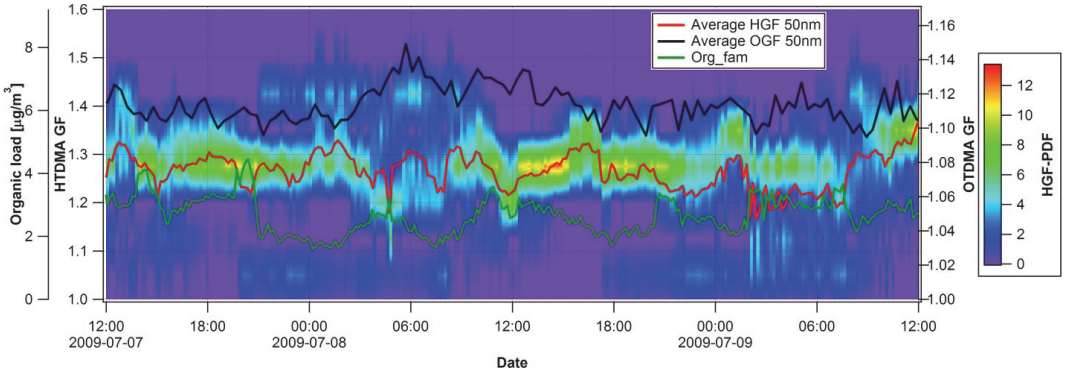

Fig. 4. Organic TDMA versus HTDMA and AMS organic load (Organic families – Org_fam) for the first period. 50 nm was chosen as it was common for both instruments.

ACPD
13, 3247–3278, 2013

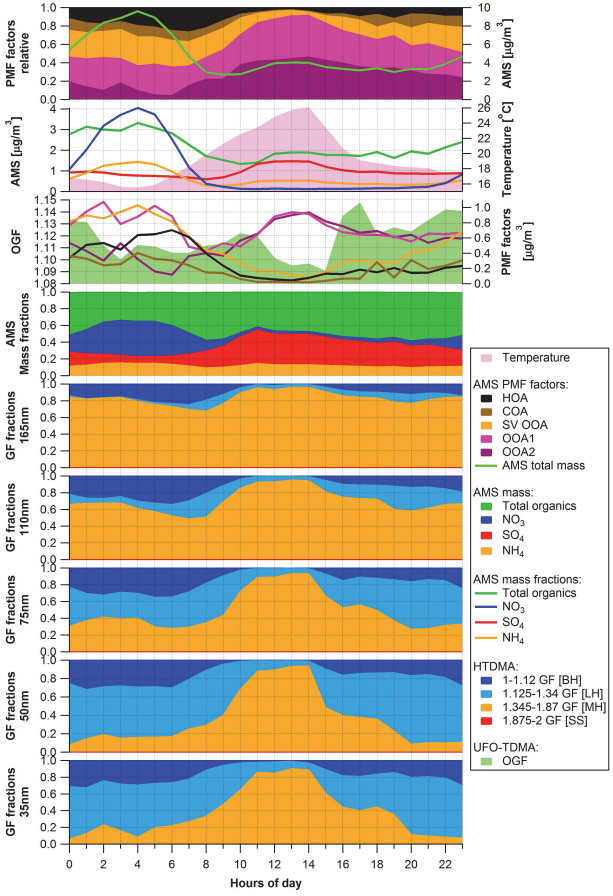

Fig. 5. Diurnal pattern for HGF, AMS mass fractions, PMF factors and temperature. Period: 9 July 2009 12:00 to 11 July 2009 12:00.

ACPD
13, 3247–3278, 2013

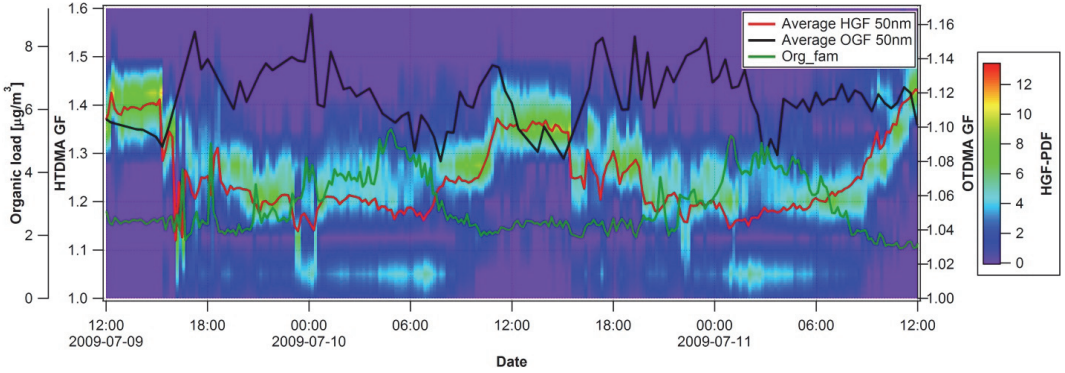

Fig. 6. Organic TDMA versus HTDMA and AMS total organic load (Organic families – Org_fam) for the second period. 50 nm was chosen as it was in common for both instruments.

ACPD
13, 3247–3278, 2013

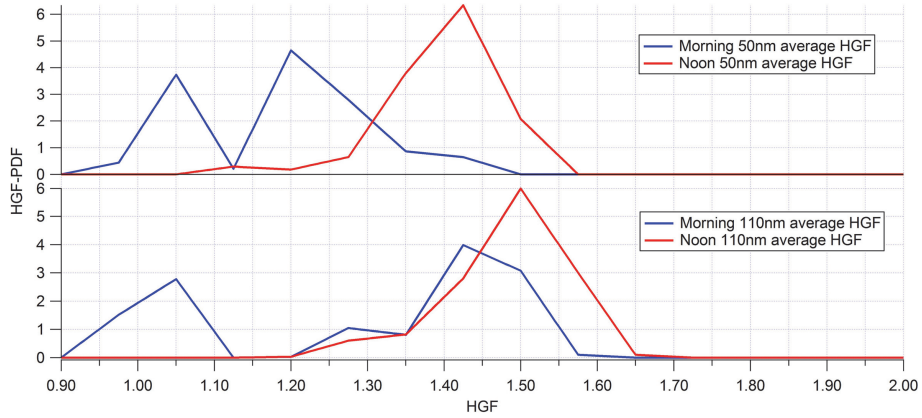

Fig. 7. HGF-PDF time slices for the morning average period (04:00–05:00) and for the noon average period (12:00–13:00) for 50 nm and 110 nm sized particles.

ACPD
13, 3247–3278, 2013

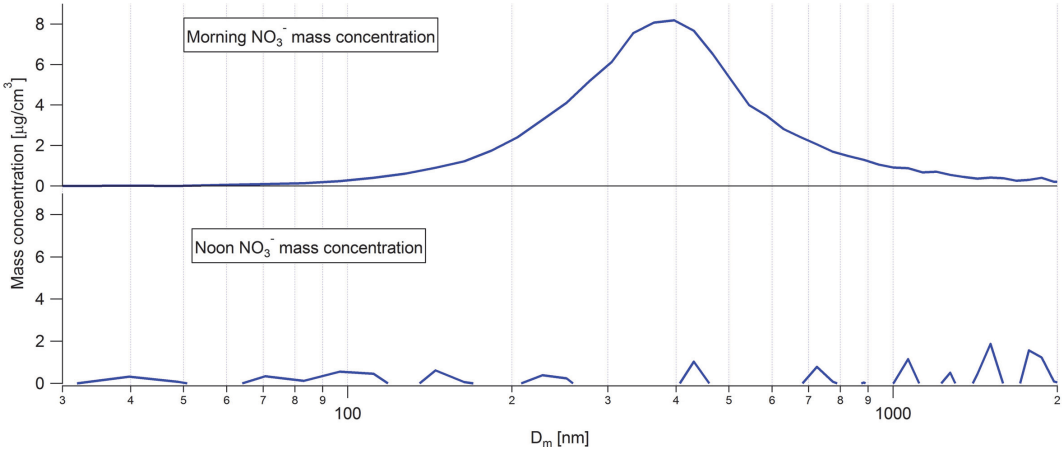

Fig. 8. AMS size-segregated mass distribution of nitrates (NO_3^-) for the morning average period (04:00–05:00) and for the noon average period (12:00–13:00) of *Case 2*.

ACPD
13, 3247–3278, 2013

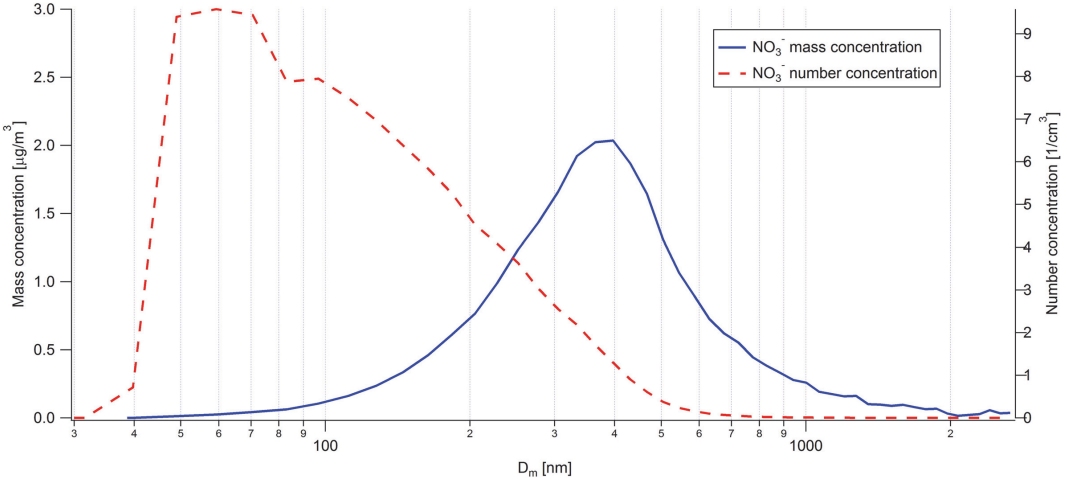

Fig. 9. AMS size segregated mass and number concentration of nitrates (NO_3^-) for *Case 2*.

ACPD
13, 3247–3278, 2013

Hygroscopic and chemical characterisation of Po Valley aerosol

J. Bialek et al.